19th Australasian Fluid Mechanics Conference
Melbourne, Australia
8-11 December 2014

Influence of a Seed Magnetic Field on the Imploding Cylindrical Richtmyer-Meshkov Instability in Magnetohydrodynamics

W. Mostert[1], V. Wheatley[1], R. Samtaney[2], and D.I. Pullin[3]

[1]School of Mechanical and Mining Engineering, University of Queensland, Queensland 4072, Australia
[2]Mechanical Engineering, King Abdullah University of Science and Technology, Thuwal, Saudi Arabia
[3]Graduate Aerospace Laboratories, 105-50, California Institute of Technology, Pasadena, CA 91125, USA

Abstract

We investigate the behaviour of the ideal magnetohydrodynamic (MHD) Richtmyer-Meshkov instability (RMI) in two-dimensional implosions under the influence of uniform- and saddle-topology seed magnetic fields. The RMI is a hydrodynamic instability that, along with the Rayleigh-Taylor instability, greatly limits the operating parameters of inertial confinement fusion (ICF), a technology that has recently seen much interest for its potential for energy production. The instability arises when a perturbed density interface is impulsively accelerated, for example by a shock wave, causing the perturbations on the interface to grow as a result of baroclinic vorticity generation. Here we present case studies of the MHD RMI in converging two-dimensional geometry, in the presence of uniform- and saddle-topology seed fields. We examine the shock refraction process, identifying the waves that result from it, and determine the growth rate of the RMI, comparing it to its behaviour in the converging hydrodynamic (no-field) case. We drive the incident shocks with a Riemann problem, and examine the RMI under various perturbation wavenumbers and seed field strengths. The shock refraction processes produce a collection of fast and sub-fast MHD shock waves which carry vorticity along and away from the interface perturbations, depending on the local field orientation to the interface, supressing the instability but leading to slightly irregular perturbation shapes. These results encourage further research on the MHD RMI in converging flows, with a strong potential for application to ICF experiments.

Introduction

Inertial Confinement Fusion (ICF) is a promising energy generation technique by which a millimetre-scale capsule, or target, filled with a deuterium-tritium fuel mixture is illuminated by high-intensity radiation, which vapourises the shell material and sends a spherical shock wave into the fuel, compressing it to temperatures and pressures where nuclear fusion may occur [5]. Its operating parameters are however limited in part by the presence of hydrodynamic instabilities such as the Rayleigh-Taylor and Richtmyer-Meshkov instability (RMI) [5].

The concept of applying a seed magnetic field to increase the performance of ICF has seen recent investigation. There is some evidence which suggests that applying a seed magnetic field to an ICF target may increase the hot spot temperature and neutron yield by means of electron confinement normal to magnetic field lines [2, 4]. Numerical results by Perkins *et al.* [11] suggest further that the fusion yield from an ICF target can be maintained at larger shell surface perturbation amplitudes in the presence of increasing seed field strength; they also observe the possibility of suppression of the Rayleigh-Taylor instability under these seed fields.

There remains the potential of suppressing the RMI in ICF by applying a seed magnetic field; its suppression is well-documented under planar flows [8, 12, 13, 10, 15], but its behaviour in cylindrical or spherical converging MHD flows under seed fields has to our knowledge yet to be investigated in detail. The cylindrical and spherical converging RMI in hydrodynamic (HD) flows is however well-understood [16], and the effect of the seed field on the symmetry of an MHD implosion has seen recent study [7].

In this study we present key examples of the converging cylindrical RMI under a single-mode sinusoidal initial perturbation in a density interface under uniform and saddle seed field configurations. These fields are examined respectively for their physical plausibility and potential to preserve symmetry in the converging flow. We characterise the types of waves formed by the shock-interface interaction in the context of prior research, and compare the growth of the interface perturbation amplitude between field configurations and the HD case.

Formulation

The variables used in this study are non-dimensionalized thus:

$$\hat{\mathbf{x}} = \frac{\mathbf{x}}{L_0}, \quad \hat{t} = \frac{t}{L_0/\sqrt{p_0/\rho_0}}, \quad \hat{\rho} = \frac{\rho}{\rho_0}, \quad \hat{p} = \frac{p}{p_0},$$
$$\hat{\mathbf{u}} = \frac{\mathbf{u}}{\sqrt{p_0/\rho_0}}, \quad \hat{\mathbf{B}} = \frac{\mathbf{B}}{\sqrt{\mu_0 p_0}}, \tag{1}$$

where $\mathbf{x}$ and t are position and time respectively; ρ is density, p pressure, $\mathbf{u}$ velocity, $\mathbf{B}$ magnetic field, μ_0 the permeability of free space, and L_0 is a reference length. 0-subscripts indicate reference values. Thus, suppressing the carets for convenience, we write the equations of ideal MHD [3], which govern the physics of the problems in this study:

$$\frac{\partial \rho}{\partial t} + \nabla \cdot (\rho \mathbf{v}) = 0, \tag{2}$$
$$\rho\left(\frac{\partial \mathbf{v}}{\partial t} + \mathbf{v} \cdot \nabla \mathbf{v}\right) + \nabla p - (\nabla \times \mathbf{B}) \times \mathbf{B} = 0, \tag{3}$$
$$\frac{\partial p}{\partial t} + \mathbf{v} \cdot \nabla p + \gamma p \nabla \cdot \mathbf{v} = 0, \tag{4}$$
$$\frac{\partial \mathbf{B}}{\partial t} - \nabla \times (\mathbf{v} \times \mathbf{B}) = 0, \quad \nabla \cdot \mathbf{B} = 0. \tag{5}$$

The model is ideal, neglecting diffusion effects - since they occur over a much larger timescale than advection effects - and gravity, and considers a continuous quasi-neutral single-fluid plasma.

To reproduce the cylindrical RMI in the converging MHD flow we define a two-dimensional (cylindrical) density interface (DI), centred at the domain origin and perturbed with a single-mode sinusoid, and accelerate it with a set of MHD shocks generated by a Riemann problem. See Figure 1 for the initial conditions. The initial DI separates an outer low-density fluid from an inner high-density fluid. We use a two-dimensional Cartesian domain, defined in x, y co-ordinates, around a z-axis. We

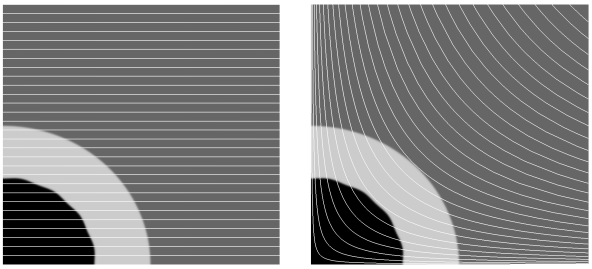

(a) Case C1 (b) Case C3

Figure 1: Initial conditions in the computational domain for cases C1 and C3 showing density field (darker is greater) with overlaid magnetic field lines.

define the radius variable as $r = \sqrt{x^2+y^2}$, with the polar angle $\phi = \arctan y/x$. The local angle between a wavevector and the magnetic field is denoted θ. The plasma is modelled with a specific heat ratio of $\gamma = 5/3$.

The density ratio across the DI is set to $\rho_1/\rho_0 = 5$, where ρ_1 is the density of the (inner) heavier fluid and ρ_0 is the reference density, set to the outer fluid. The DI is regularised with an hyperbolic tangent function and has an initial interface profile given by

$$r_i(\phi) = r_0 + \eta_0 \cos(k\phi), \tag{6}$$

with k and η_0 being the perturbation wavenumber and initial amplitude respectively. The initial amplitude in this study is set to 2% the wavelength λ, and we consider wavenumbers $k = 16, 64$.

A Riemann problem describes the flow resulting from an initial discontinuous separation of two uniform states, and in converging MHD flows thus produces a complete set of converging fast and slow MHD shocks. We place the driving Riemann interface (RI), also regularised and centred at the domain origin, at $r_d = 1.6$, providing a discontinuity in pressure and density. The inside pressure and density are set to their respective reference values, p_0 and ρ_0. The outside pressure and density are $\rho_d = 3\rho_0$ and $p_d = 12.1 p_0$ respectively.

As the measure of magnetic field strength we use $\beta_{0I} = 2p_0/B_0^2$, where the subscript I indicates the use of the reference pressure, which exists inside the RI, and subscript 0 indicates the initial value at the mean DI radius, r_0. For this study we set $\beta_{0I} = 4$.

Two kinds of magnetic field configurations are applied across this domain denoted C1 and C3:

C1: Uni-direction field in cylindrical geometry
This is a uniform field, set to the reference strength:

$$\mathbf{B} = B_0 \hat{\mathbf{e}}_\mathbf{x}. \tag{7}$$

C3: Saddle field in cylindrical geometry
This field presents a saddle configuration in the domain and is defined by:

$$\mathbf{B}(x,y) = \sum_{i=1}^{4} \left\{ \frac{\alpha_i B_0}{(x-x_i)^2 + (y-y_i)^2} \left[-(y-y_i)\hat{\mathbf{e}}_\mathbf{x} + (x-x_i)\hat{\mathbf{e}}_\mathbf{y} \right] \right\}, \tag{8}$$

where $\alpha_i = \{+\alpha_0, -\alpha_0, -\alpha_0, +\alpha_0\}$ is a signed scaling parameter that sets $|B(r_0)| = B_0$; and $(x_i, y_i) = \{(10,10), (-10,10), (-10,-10), (10,-10)\}$.

Methodology

The flows are solved numerically with a second-order accurate, non-linear compressible finite volume code developed by Samtaney [9] for solving the ideal MHD equations using a dimensionally unsplit upwinding scheme and a Roe-type flux solver, with a projection method used to enforce a solenoidal magnetic field. We use an adaptive mesh refinement scheme of the Berger-Collela type under the Chombo framework.

The mesh is a uniform cartesian grid with an unrefined resolution of 256^2 with three levels of refinement of ratio 2 in each direction. The criterion for refinement is $|\nabla\rho| > 0.02\rho$ on the local ρ, so that the effective resolution is 2048^2 on the compressible flow features. We discretize on a quarter-domain of the flow, $0 < x, y < l$ where $l = 3$.

Results

Figure 2 shows the HD and MHD RMI, the latter in a configuration of C1 under a reference field strength $\beta_{0I} = 4$, for a wavenumber of $k = 16$ at some time after the initial shock has processed the DI, visualising density gradient. The perturbations on the DI have grown much more in the HD flow than in the MHD flow, implying suppression of the RMI in the presence of a seed magnetic field. Note that while the perturbation growth is axisymmetric in the HD case, it is not in the MHD case, with the perturbations at polar angle $\phi = \pi/2$ appearing much flatter than at $\phi = 0$. We will now characterise this flow as a case study, and afterwards move onto additional formulations to examine differences between initial wavenumbers and field configurations.

The driving shocks are generated by the Riemann problem, and are characterised according to previous study [6] - that is, moving from the inside outward, there is a fast magnetosonic shock, a slow magnetosonic shock, a contact interface (that is, a discontinuity in density but not pressure, equivalent to the DI), a slow magnetosonic expansion, and a fast magnetosonic expansion. The two waves of interest are the fast and slow shocks; these process the DI at different times and in different manners, and we examine their respective contributions in order.

In studies investigating the HD RMI, only one driving shock typically exists, and this shock is axisymmetric (or in the case of spherical flow, spherisymmetric). In this flow, the incident fast shock (IFS) plays a similar role to the shock in HD studies, except that its strength and geometry varies slightly with the field orientation to the shock normal, θ. This loss of symmetry is due to the presence of the magnetic field [7]. Note that the fast shock does not then process the entire DI at once. Furthermore,

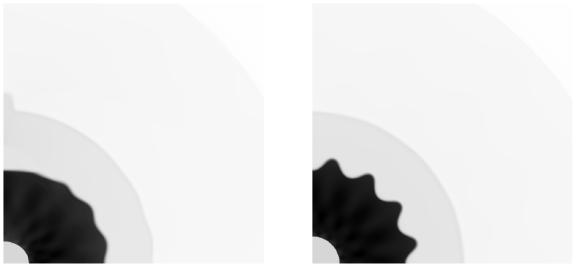

(a) Case C1 (b) Case HD

Figure 2: Developed density field for C1 configuration and the no-field (HD) cases at $t \simeq 0.71$, for $k = 16$ (darker is greater).

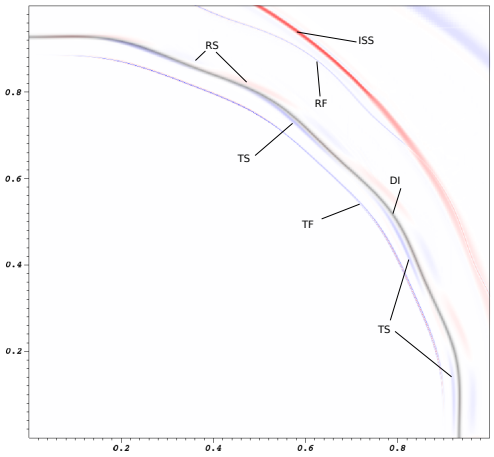

Figure 3: Refraction of the IFS through the DI, under a C1 field configuration, $\beta = 4$, $k = 16$ at $t \simeq 0.29$. Coloured waves are shocks, visualised in vorticity, and grey is the DI.

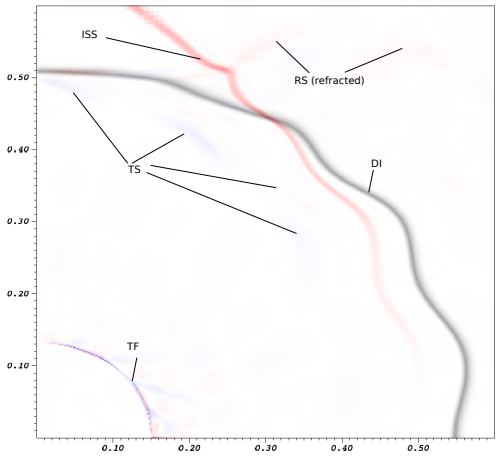

Figure 4: Refraction of the ISS through the DI, under a C1 field configuration, $\beta = 4$, $k = 16$, at $t \simeq 0.71$. Coloured waves are shocks, visualised in vorticity, and grey is the DI.

as the shock processes the DI it generates a series of transmitted and reflected waves. These can be seen in Figure 3, and are as follows, following the nomenclature of Wheatley *et al.* [12]:

1. TF - a transmitted fast shock; this is equivalent to the transmitted shock in an HD RMI flow;
2. TS - a transmitted sub-fast shock; this wave carries vorticity away from the DI along the local magnetic field lines. This wave is difficult to capture, is quite diffuse, and is not strongly compressive;
3. RS - similar to the TS, this is a reflected sub-fast shock which carries vorticity away from the DI;
4. RF - similar to the TF, this is a fast shock and is equivalent to the reflected shock in an HD RMI flow. In this flow it is well-resolved but not strongly compressive.

The direct mechanism of suppression of the RMI is the combination of the sub-fast waves TS and RS, which carry vorticity away from the DI. This suppression mechanism has been noted in previous research [13]. Note however that at orientations where the field is parallel or nearly parallel to the DI, these sub-fast waves travel along the DI. This is in line with Wheatley *et al.*, who observed this phenomenon via simulations of the planar transverse field case [15]. These waves do not, however, promote growth of the perturbations on the DI since they continually interfere constructively and destructively with each other, causing the interface perturbations to oscillate.

The incident slow shock (ISS) processes the DI differently; it is more diffuse (numerically) than the incident fast shock (IFS), and changes in its compressiveness dramatically between $\theta = 0$, where it has near-zero strength and is close to the incident fast shock, and $\theta = \pi/2$, where it is close to the contact interface resulting from the Riemann problem.

Before the ISS can reach the DI, it must first traverse the reflected waves RF and RS. It produces an additional wave, which appears to be an additional reflected slow shock, on interacting with the RF, and is weakened and slowed by the interaction with the RS, while RS itself weakens and refracts strongly toward the normal of the ISS. At this point, the ISS is quite slow and has a low speed relative to the DI; as a result, it passes through the DI very gradually - see Figure 4. Unlike the IFS, however, the ISS

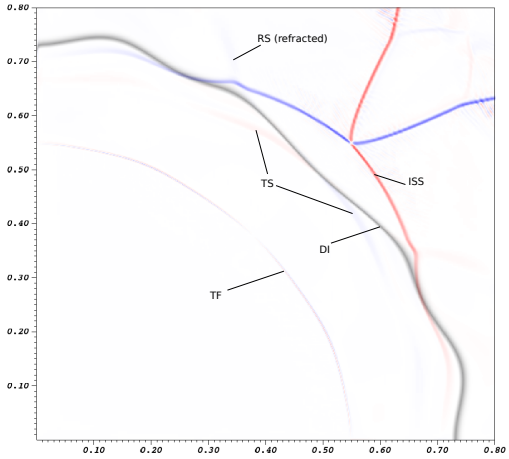

Figure 5: Refraction of the ISS through the DI under a C3 field configuration, $\beta_0 = 4$, $k = 16$, at $t \simeq 0.57$. Coloured waves are shocks, visualised in vorticity, and grey is the DI.

does not interact strongly with the DI: the baroclinically generated vorticity and additional waves resulting from the interaction are too weak to be visible in these results. It does refract slightly as it moves into the denser fluid inside the DI.

At late times, the contact point between the ISS and the DI moves towards the polar angle $\phi = \pi/2$, where a singularity in the slow shock geometry ("kink") exists [6]. The formulation of the problem is such that by the time this singularity approaches the DI closely, the TF is about to re-process the DI, having reflected off the domain centre, in a process called reshock. We therefore do not consider the interaction of the kink with the DI.

Figure 5 shows the wave structure for C3 at $t \simeq 0.45$, as the ISS is processing the DI. This is equivalent to the ISS processing the DI in C1, shown in Figure 4. Similar flow structures to case C1 appear, but with double the azimuthal frequency.

Figure 6 compares maximum perturbation amplitude and compression ratio (calculated from the mean DI radius) between the C1, C3, and HD cases for two wavenumbers $k = 16, 64$. For the C1 and C3 cases, only the largest amplitude in the domain is presented; these amplitudes are associated with the wavelengths where the field is normal to the DI, that is at polar angles $\phi \simeq 0$.

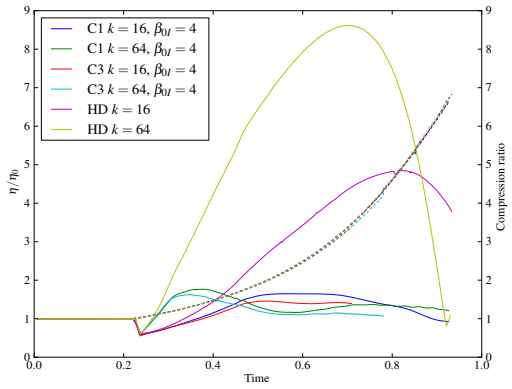

Figure 6: Normalised maximum perturbation amplitude (solid) and compression ratio (dashed) for no-field (HD), uniform-field (C1) and saddle field (C3) configurations, with wavenumber k.

The seed-field cases show perturbation amplitudes that are universally lower than the corresponding no-field cases, suggesting suppression of the RMI. The amplitudes in fact begin to decrease after some time due to the inward acceleration of the surrounding flow, causing the onset of the Rayleigh-Taylor instability. These negative growth rates are, however, far smaller than in the HD cases, indicating the RTI is also suppressed by the seed field. High wavenumbers see a high and consistent initial growth independent of field strength or configuration; this is characteristic of the RMI, whose (early) linear growth rate is proportional to wavenumber [1]. C3 fields consistently achieve lower peak perturbation amplitude than their C1 counterparts. The compression ratio appears unaffected by field configuration, strength, or perturbation wavenumber, and does not reach any maximum for these simulation times.

Due to the wavelengths represented in these amplitude graphs existing at very low ϕ, the effect of the ISS is not visible in Figure 6, since the ISS weakens to zero strength at $\theta = \phi = 0$.

Conclusion

We examine the Richtmyer-Meshkov instability (RMI) in two-dimensional converging cylindrical magnetohydrodynamic (MHD) flows, under a seed magnetic field. For the field configurations and initial perturbation wavenumbers tested, the RMI is suppressed, showing an initial linear growth rate, as in the hydrodynamic (HD) case, followed by a subsequent decrease which we attribute to the transport of vorticity; we note that a saddle-field configuration shows increased suppression over the uniform-field case, while increased perturbation wavenumber gives a higher initial growth rate and peak amplitude. The converging MHD shocks process the material interface in different ways - the first accelerating shock, a fast MHD shock, produces four transmitted and reflected waves, as expected from previous studies on the planar MHD RMI; the slower of these waves serve to carry vorticity away away from the material interface, suppressing its growth. The second incident shock, a slow MHD shock, refracts through the material interface but does not appear to dramatically affect its growth characteristics.

Acknowledgements

This research was supported under Australian Research Council's Discovery Projects funding scheme (project number DP120102378). W. Mostert is supported by an Australian Postgraduate Award. Dr Wheatley is the recipient of an Australian Research Council Discovery Early Career Researcher Award (project number DE120102942). Prof. Samtaney is partially support by a KAUST Base Research Award.

References

[1] Brouillette, M., The Richtmyer-Meshkov instability, *Annual Review of Fluid Mechanics*, **34**, 2002, 445–468.

[2] Chang, P. Y., Fiksel, G., Hohenberger, M., Knauer, J. P., Betti, R., Marshall, F. J., Meyerhofer, D. D., Séguin, F. H. and Petrasso, R. D., Fusion yield enhancement in magnetized laser-driven implosions, *Phys. Rev. Lett.*, **107**, 2011, 035006.

[3] Goedbloed, J., Keppens, R. and Poedts, S., *Advanced Magnetohydrodynamics*, Cambridge University Press, 2010.

[4] Hohenberger, M., Chang, P.-Y., Fiksel, G., Knauer, J. P., Betti, R., Marshall, F. J., Meyerhofer, D. D., Sguin, F. H. and Petrasso, R. D., Inertial confinement fusion implosions with imposed magnetic field compression using the omega laser, *Physics of Plasmas*, **19**, 2012, –.

[5] Lindl, J. D., Amendt, P., Berger, R. L., Glendinning, S. G., Glenzer, S. H., Haan, S. W., Kauffman, R. L., Landen, O. L. and Suter, L. J., The physics basis for ignition using indirect-drive targets on the national ignition facility, *Physics of Plasmas*, **11**, 2004, 339–491.

[6] Mostert, W., Wheatley, V., Hingee, M. and Samtaney, R., The cylindrical Riemann problem in magnetohydrodynamics: A case study, in *18th Australasian Fluid Mechanics Conference*, 2012.

[7] Mostert, W., Wheatley, V., Samtaney, R. and Pullin, D. I., Effects of seed magnetic fields on magnetohydrodynamic implosion structure and dynamics, *Physics of Fluids*, submitted/under review.

[8] Samtaney, R., Suppression of the Richtmyer-Meshkov instability in the presence of a magnetic field, *Physics of Fluids*, **15**, 2003, L53–L56.

[9] Samtaney, R., Colella, P., Ligocki, T. J., Martin, D. F. and Jardin, S. C., An adaptive mesh semi-implicit conservative unsplit method for resistive mhd, *Journal of Physics: Conference Series*, **16**, 2005, 40.

[10] Wheatley, V., Gehre, R., Samtaney, R. and Pullin, D. I., The magnetohydrodynamic Richtmyer-Meshkov instability: The oblique field case, in *29th International Symposium on Shock Waves*, 2013.

[11] Perkins, L. J., Logan, B. G., Zimmerman, G. B., and Werner, C. J., Two-dimensional simulations of thermonuclear burn in ignition-scale inertial confinement fusion targets under compressed axial magnetic fields," *Physics of Plasmas*, **20**, 2013, 072708.

[12] Wheatley, V., Pullin, D. I. and Samtaney, R., Regular shock refraction at an oblique planar density interface in magnetohydrodynamics, *Journal of Fluid Mechanics*, **522**, 2005, 179–214.

[13] Wheatley, V., Pullin, D. I. and Samtaney, R., Stability of an impulsively accelerated density interface in magnetohydrodynamics, *Phys. Rev. Lett.*, **95**, 2005, 125002.

[14] Wheatley, V., Samtaney, R. and Pullin, D. I., The Richtmyer-Meshkov instability in magnetohydrodynamics, *Physics of Fluids*, **21**, 2009, –.

[15] Wheatley, V., Samtaney, R., Pullin, D. I. and Gehre, R. M., The transverse field Richtmyer-Meshkov instability in magnetohydrodynamics, *Physics of Fluids*, **26**, 2014, –.

[16] Zhang, Q. and Graham, M. J., A numerical study of Richtmyer-Meshkov instability driven by cylindrical shocks, *Physics of Fluids*, **10**, 1998, 974–992.